

Article

Open Access



Hierarchical Ni- and Co-based oxynitride nanoarrays with superior lithiophilicity for high-performance lithium metal anodes

Yaya Wang¹, Hanjiao Xu¹, Jiang Zhong¹, Tao Wang¹, Bingan Lu², Jian Zhu¹, Xidong Duan¹

¹State Key Laboratory for Chemo/Biosensing and Chemometrics, College of Chemistry and Chemical Engineering, Hunan Key Laboratory of Two-Dimensional Materials, Engineering Research Center of Advanced Catalysis, Ministry of Education, Hunan University, Changsha 410082, Hunan, China.

²School of Physics and Electronics, Hunan University, Changsha 410082, Hunan, China.

Correspondence to: Prof. Jian Zhu, College of Chemistry and Chemical Engineering, Hunan University, 2 Lushan South Road, Changsha 410082, Hunan, China. E-mail: jzhu@hnu.edu.cn; Prof. Xidong Duan, College of Chemistry and Chemical Engineering, Hunan University, 2 Lushan South Road, Changsha 410082, Hunan, China. E-mail: xidongduan@hnu.edu.cn

How to cite this article: Wang Y, Xu H, Zhong J, Wang T, Lu B, Zhu J, Duan X. Hierarchical Ni- and Co-based oxynitride nanoarrays with superior lithiophilicity for high-performance lithium metal anodes. *Energy Mater* 2021;1:100012. <https://dx.doi.org/10.20517/energymater.2021.18>

Received: 10 Oct 2021 **First Decision:** 25 Oct 2021 **Revised:** 31 Oct 2021 **Accepted:** 5 Nov 2021 **Published:** 18 Nov 2021

Academic Editors: Yuping Wu, Hao Liu **Copy Editor:** Yue-Yue Zhang **Production Editor:** Yue-Yue Zhang

Abstract

Lithium metal has emerged as the most prospective candidate for the realization of improved battery systems. However, notorious Li dendrite formation and the huge volume effect during cycling critically impair the further practical deployment of Li metal batteries. Herein, we propose hierarchical Ni- and Co-based oxynitride (NiCoO₂/CoO/Ni₃N) nanoarrays with superior lithiophilicity on a three-dimensional nickel foam (NiCoON/NF) as a host for highly stable Li metal anodes. The uniform nitrogen-infused nanorod-on-nanosheet arrays present improved electrical conductivity and an increased concentration of active sites with oxygen vacancies to enhance the surface lithiophilicity, which effectively facilitates homogeneous Li nucleation/growth. Moreover, the hyperbranched structure can induce a homogeneous distribution of Li-ion flux, owing to the enlarged surface area, thereby providing sufficient space to store deposited lithium and relieve the volume expansion. Consequently, the NiCoON/NF host delivers a high Coulombic efficiency (98.4% over 600 cycles) at 1 mA cm⁻² and an ultralong lifespan (> 2000 h) under a high capacity of 3 mAh cm⁻². Remarkably, a Li@NiCoON/NF-LiFePO₄ full battery also reveals impressive electrochemical performance. This work demonstrates new insights into safe rechargeable Li metal batteries.



© The Author(s) 2021. **Open Access** This article is licensed under a Creative Commons Attribution 4.0 International License (<https://creativecommons.org/licenses/by/4.0/>), which permits unrestricted use, sharing, adaptation, distribution and reproduction in any medium or format, for any purpose, even commercially, as long as you give appropriate credit to the original author(s) and the source, provide a link to the Creative Commons license, and indicate if changes were made.



Keywords: Hyperbranched structure, lithiophilic oxynitride nanoarrays, high Coulombic efficiency, super cycling stability, lithium metal anodes

INTRODUCTION

With the intensive demand for electric vehicles and a wide range of intelligent machines, high energy density storage technologies are attracting extensive interest, driven by their long cycle life and ultrahigh power^[1-4]. Lithium metal is an excellent choice as an anode for next-generation batteries due its high specific capacity (3860 mAh g⁻¹) and ultralow redox potential (-3.04 V vs. a standard hydrogen electrode)^[5,6]. Nevertheless, the irregular Li dendrites and inevitable volume variation associated with lithium metal anodes result in internal short circuit and severe safety risks^[7,8]. Meanwhile, the continuous breakdown/reconstruction of the solid electrolyte interphase (SEI) during repeated Li plating/stripping can cause poor Coulombic efficiency (CE) due to the constant consumption between the electrolyte and the newly exposed fresh Li^[9]. All these problems deeply restrict the deployment of lithium metal batteries.

So far, multiple strategies have been reasonably put forward to address the above hurdles, including the construction of stable solid electrolyte interphase layers via electrolyte engineering^[10-13], optimization of the functional separator and the design of solid-state or gel-polymer electrolytes^[14-19]. Although clear achievements have been made regarding interfacial modification, the volume effect still limits the commercialization of lithium metal anodes. Notably, three-dimensional (3D) porous hosts with specific lithiophilic nanostructures have emerged as attractive alternatives to promote homogeneous Li nucleation/growth and accommodate the volume changes^[20-23]. For example, Lu *et al.*^[24] reported a lithiophilic NiO hexagonal plate on a Ni substrate to boost uniform lithium deposition. Wang *et al.*^[25] developed hierarchical nanosheet arrays of metal oxides to effectively stimulate Li-ion redistribution. Huang *et al.*^[26] found that the fabrication of lithiated NiCo₂O₄ nanorods on a Ni matrix can reduce the average electrical current, leading to significantly improved electrochemical performance. These contributions indicate that the design of densely vertical architectural arrays on a planar/3D host could be highly efficient in suppressing Li dendrites. However, the main drawback of metal oxides is their poor electronic conductivity, which could be undesirable for achieving dendrite-free Li anodes.

Nitrogen doping can create a nitrogen-rich surface as an effective approach to boost conductivity and enable improved lithiophilicity of oxygen species and electrochemical performance^[27,28]. Recently, plasma-enhanced strategies have been adopted to produce nitrogen-doped CuO nanosheets with high lithiophilicity on Cu foil and metal nitride-decorated Ni foam^[29,30]. Ammonia calcination methods have also been used to prepare CuON and Co₃N on 3D Cu/Ni foam to enhance the lithiophilicity and electronic conductivity to achieve even Li deposition^[31,32]. Ni- and Co-based oxynitrides with certain levels of oxygen vacancies after the treatment with NH₃ can produce enhanced electrical conductivity and increased active sites^[33,34]. Therefore, the development of Ni- and Co-based oxynitrides as anodes for advanced lithium metal batteries is a highly promising approach.

Here, we present a hierarchical NiCoO₂/CoO/Ni₃N nanoarray (abbreviated as NiCoON)-decorated 3D Ni foam (NiCoON/NF) produced via a facile in situ hydrothermal and nitriding approach as a current collector for stable Li metal anodes. Compared with its NiCo₂O₄ counterpart, the newly obtained NiCoON/NF nanocomposite consisting of a significant level of oxygen vacancies shows significant improvements in electronic/ionic conductivity and more active sites to enhance surface lithiophilicity, which can reduce the nucleation barrier. Moreover, the hierarchical architecture, including vertical nanorod-on-nanosheet arrays, offers an enlarged surface area to ensure a uniform distribution of Li-ion

flux. Therefore, the 3D NiCoON/NF host achieves a reduced overpotential of 22 mV, a high CE of 98.4% (600 cycles) and excellent cycling behavior (2000 h). Furthermore, the Li@NiCoON/NF-LiFePO₄ full battery also presents a long lifespan for continuous 400 cycles at 1 C (160 mA g⁻¹).

EXPERIMENTAL

Preparation of NiCoON/NF current collector

NiCoON/NF was prepared by a hydrothermal method and subsequent ammoniation. The surface oxides of the Ni foam were removed by immersion in hydrochloric acid, followed by ultrasonic cleaning with acetone, water and ethanol sequentially. 2.62 mmol Co(NO₃)₂·6H₂O, 1.31 mmol Ni(NO₃)₂·6H₂O, 26.25 mmol urea and 10.5 mmol NH₄F were dissolved in 70 mL of deionized water by stirring and mixing well at room temperature and then transferred to a 100 mL Teflon-lined stainless-steel autoclave. The pretreated Ni foam (2 cm × 4 cm) was vertically immersed into the reaction solution and annealed at 100 °C for 8 h. The sample was then removed and the residual impurities on the surface washed away with deionized water and ethanol successively. The prepared Ni-Co precursor was directly calcined in a NH₃ atmosphere with a constant temperature of 350 °C for 3 h, with a heating rate of 2 °C min⁻¹ to obtain an oxynitride nanoarray on the Ni foam (NiCoON/NF). For the fabrication of NiCoO, the Ni-Co precursor was heated and calcined at 350 °C in an air atmosphere for 1 h to obtain the NiCoO sample on the Ni foam (NiCoO/NF).

Materials characterization

The surface and cross-sectional morphologies were observed using a field-emission S4800 instrument (Zeiss, Germany). The elemental mappings were captured using energy-dispersive X-ray spectroscopy. The high-resolution transmission electron microscopy (HRTEM) image was taken using a JEOL JEM-2100F. X-ray photoelectron spectroscopy (XPS) was carried out to obtain the surface chemical elements using a K-Alpha ESCALAB 250Xi system. All peaks were calibrated based on the C 1s peak (284.8 eV). X-ray diffraction (XRD) patterns were collected to analyze the phase composition on an XRD-6100 diffractometer coupled with Cu-Kα radiation (Shimadzu, Japan). The pore structure distributions and surface areas from the Brunauer-Emmett-Teller (BET) method were detected using an absorption analyzer (Micromeritics ASAP 2020) and N₂ adsorption-desorption isotherm at 77 K.

Electrochemical measurements

CR2032-type coin cells were used to assemble lithium metal batteries with Li as the reference and NiCoON/NF, NiCoO/NF or NF as the working electrode, where the water and oxygen contents were required to be less than 0.5 ppm. 1 M LiTFSI dissolved in 1,3-dioxolane/1,2-dimethoxyethane (v:v = 1:1) with 2 wt.% LiNO₃ and polypropylene (Celgard 2400) were selected as the electrolyte and separator, respectively. Before testing, all assembled batteries were activated for five cycles under a voltage window of 0.01-1.0 V to remove the contaminants at 50 μA and stabilize the SEI. To investigate the CE, a certain amount of lithium (1 mAh cm⁻²) was plated onto different working electrodes, followed by charging up to 1 V to facilitate the release of Li at several current densities (1, 2 and 5 mA cm⁻²). The CE was also tested under a higher areal capacity of 3 mAh cm⁻² with 1 mA cm⁻² and 2 mAh cm⁻² with 2 mA cm⁻². For the symmetrical cell, 3 mAh cm⁻² of Li was pre-electroplated on NF, NiCoO/NF and NiCoON/NF, followed by galvanostatic charge and discharge at 1 and 5 mA cm⁻² for 1 mAh cm⁻². With a higher areal capacity of 3 mAh cm⁻² at 1 mA cm⁻², the voltage hysteresis was also measured. All electrochemical properties were measured on multichannel LAND-CT2001A battery test equipment.

For the performance test of the full battery, NiCoON/NF, NiCoO/NF and NF were used as substrates for pre-lithiation to obtain Li@NiCoON/NF, Li@NiCoO/NF and Li@NF as anodes, respectively. Commercial LiFePO₄ was chosen as the stable cathode material. LiFePO₄ powder, Super P and polyvinylidene difluoride

at a mass ratio of 80:10:10 were mixed in a N-methyl-2-pyrrolidone solvent, followed by continuous stirring overnight. The homogeneous slurry was coated onto clean aluminum foil and the solvent was removed in a vacuum environment at 80 °C for 12 h with an area loading of 3.5 mg cm⁻². The corresponding full cells were charged and discharged between 2.4 and 4.2 V.

RESULTS AND DISCUSSION

Preparation and structure of NiCoON/NF

NiCoON/NF was obtained by a typical hydrothermal method and subsequent ammoniation [Figure 1]. The Ni-Co precursor was first in situ grown on Ni foam through a hydrothermal process. After the low-temperature ammoniating treatment, the hydroxide was converted into a NiCoO₂/CoO/Ni₃N nanocomposite (abbreviated as NiCoON). As shown in Supplementary Figure 1, the bare Ni foam shows a smooth and flat surface with an open porous structure. The XRD pattern in Supplementary Figure 2 displays characteristic peaks. An interesting architecture with nanorod-on-nanosheet arrays was uniformly deposited onto a 3D Ni skeleton [Supplementary Figure 3]. After ammoniation, the morphologies of the Ni-Co precursor were well inherited. As shown in Figure 2A, the NiCoON/NF exhibits a rough surface. The high-resolution scanning electron microscopy (SEM) images in Figure 2B and C show a well-maintained nanorod-on-nanosheet structure with a unique hyperbranched architecture, which can afford sufficient sites for lithium nucleation and a large electroactive surface area for Li plating/stripping. The corresponding EDS elemental mapping of NiCoON/NF confirms the homogeneous distribution of elemental Ni, Co, O and N throughout the nanoarray matrix, indicating the successful implantation of nitrogen species [Supplementary Figure 4].

The TEM image in Figure 2D further reveals a typical piece of the nanorod-on-nanosheet structure. From the HRTEM [Figure 2E], three well-resolved lattice intervals of 0.244, 0.214 and 0.246 nm can be ascribed to the (111) plane of rock-salt NiCoO₂, the (002) plane of hexagonal Ni₃N and the (111) plane of cubic CoO, respectively, proving the co-existence of NiCoO₂, CoO and Ni₃N. The formation of the NiCoON nanocomposite was further confirmed by the XRD patterns in Figure 2F. The typical diffraction peaks of NiCoO₂ (JCPDS 10-0188), CoO (JCPDS 48-1719) and Ni₃N (JCPDS 10-0280) are also consistent with the TEM findings. For comparison, the SEM images of NiCoO/NF prepared by calcination under air at 350 °C reveal a similar hierarchical nanostructure and uniform elemental distribution [Supplementary Figure 5]. However, no nitride peak in the XRD pattern of NiCoO/NF is found, corresponding with the TEM findings [Supplementary Figure 6]. In addition, the measured BET surface area of the NiCoON nanoarrays is 107.8 m² g⁻¹ [Supplementary Figure 7], which is larger than that of NiCoO (101.2 m² g⁻¹). Furthermore, NiCoON presents a wide range of pore size distributions from 2 to 30 nm. These results show that NiCoON/NF with a large specific surface area can effectively reduce the local current density and guide the uniform distribution of lithium ions.

XPS was performed to determine the composition and chemical states of the as-synthesized NiCoON/NF. The corresponding full-scan spectra contain elemental Ni, Co, O and N, consistent with the EDS results [Supplementary Figure 8A]. Figure 2G exhibits the high-resolution Ni 2p XPS spectrum containing Ni³⁺ (856.6 eV) and Ni²⁺ (854.8 eV), corresponding to Ni 2p_{3/2} and Ni 2p_{1/2}, respectively^[35]. Importantly, an obvious peak of Ni⁺ (853.1 eV) is found in NiCoON/NF, indicating the partial reduction of Ni²⁺ to Ni⁺ after the nitrating treatment. The N 1s spectrum clarifies the existence of Ni₃N [Figure 2I]^[36]. Furthermore, the fitted O 1s spectrum shows three characteristic peaks and the peak at 530.9 eV corresponds to the oxygen defect/vacancy species [Figure 2H]^[37,38]. The Co 2p peaks of the NiCoON/NF composite show two more obvious central satellite peaks, indicating that some Co³⁺ were reduced to Co²⁺ and formed oxygen vacancies [Supplementary Figure 8B]^[39]. Compared to NiCoON/NF, no N element or Ni⁺ (853.1 eV) peak was found

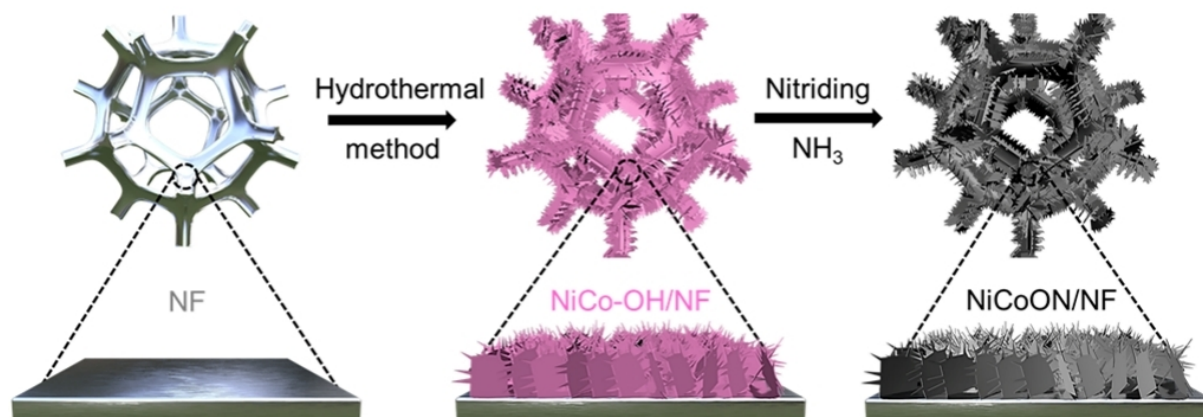


Figure 1. Schematic of preparation procedure of NiCoON/NF.

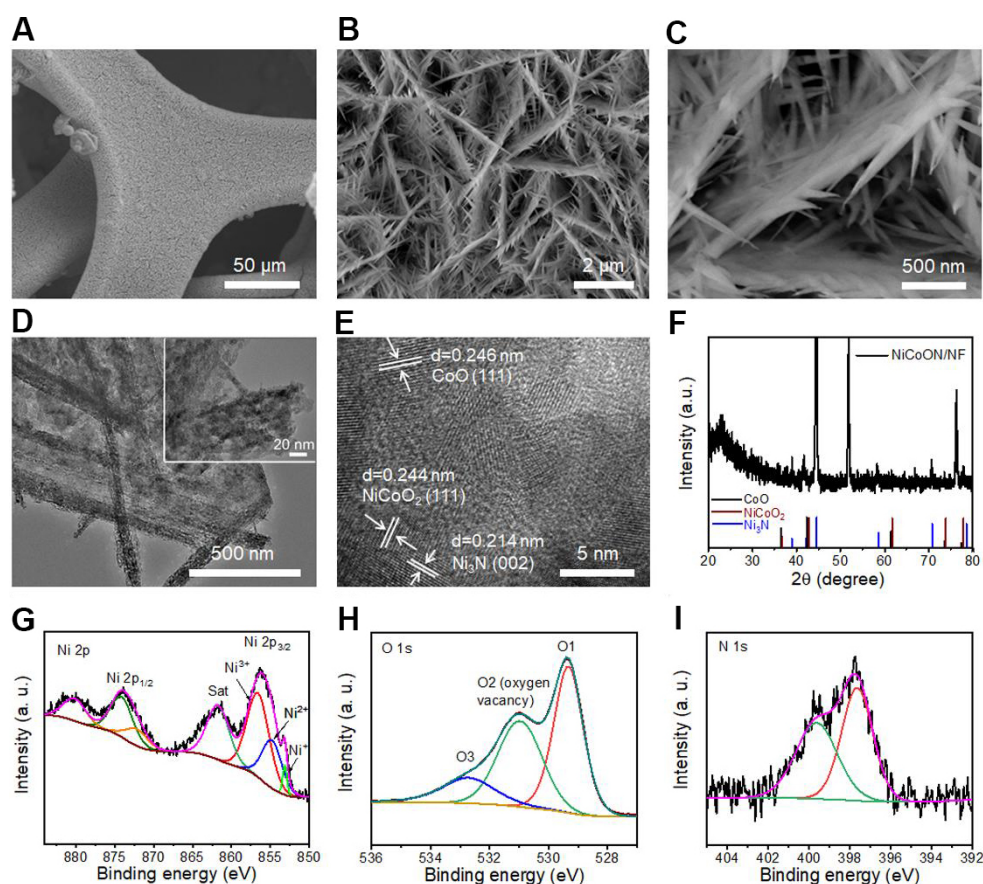


Figure 2. (A-C) SEM images of NiCoON/NF host. (D) Low-magnification and (E) high-resolution TEM images of NiCoON/NF. (F) XRD pattern of NiCoON/NF. (G) Ni 2p, (H) O 1s and (I) N 1s XPS spectra of NiCoON/NF. SEM: Scanning electron microscopy; TEM: transmission electron microscopy; XRD: X-ray diffraction; XPS: X-ray photoelectron spectroscopy.

in the full-scan spectra of NiCoO/NF and the high-resolution Ni 2p XPS spectrum [Supplementary Figure 9], respectively. The corresponding oxygen defect/vacancy species at 531.4 eV in the O 1s spectrum of NiCoO/NF is also smaller than that of NiCoON/NF and the Co 2p peak of NiCoO/NF showed no visible satellite peaks. In general, N element is successfully introduced and the concentration of

oxygen defect sites increases after the nitriding treatment, which can help to enhance the conductivity and lithiophilicity.

Electrochemical performance of NiCoON/NF

To better evaluate the electrochemical features of NiCoON/NF, the CE was tested via the assembly of half cells using Li as the reference electrode. As depicted in [Figure 3A](#), NiCoON/NF shows the lowest nucleation overpotential of only 22 mV, much lower than that of NiCoO/NF (32 mV) and bare NF (42 mV) at a current density of 1 mA cm⁻². This clearly evidences that the strong lithiophilicity of NiCoON/NF is favorable for guiding the uniform Li nucleation. [Figure 3B](#) illustrates the CE comparison among the three samples. The NiCoON/NF host exhibits an inferior value of ~93.7% in the first cycle, which may be due to the conversion reaction between Li and NiCoON. This gradually rises to > 98% upon subsequent cycles and maintains stable cycling for 600 cycles. Compared with the published studies in [Supplementary Table 1](#), such a CE is one of the best for 3D hierarchical hosts. In contrast, the CE of NiCoO/NF suffers from a sharp decline after 300 cycles, while bare NF shows a poor CE with huge fluctuations after 100 cycles due to the large consumption of electrolyte and lithium metal.

When the applied current density is increased to 2 mA cm⁻², the NiCoON/NF electrode still shows stable values of > 98% after 400 cycles, while the NiCoO/NF and NF are still in a state of poor CE [[Figure 3C](#)]. In addition, the corresponding discharge-charge curves of the NiCoON/NF host fit well with the CE and show a low nucleation overpotential in the first cycle. The voltage hysteresis is smaller than that of bare NF in the subsequent cycles, indicating the excellent stability of NiCoON/NF [[Figure 3D and E](#)]. Furthermore, even at a higher current density of 5 mA cm⁻², the NiCoON/NF still exhibits an excellent CE, while the NiCoO/NF and bare NF present severe fluctuations [[Figure 3F](#)]. Such excellent cycling stability of the NiCoON/NF electrode is mainly attributed to the formation of a stable SEI and the successful suppression of lithium dendrites.

Impressively, when the deposition capacity is substantially increased to 3 mAh cm⁻², NiCoON/NF achieves a stable CE at 1 mA cm⁻² for 160 cycles [[Supplementary Figure 10](#)]. Similarly, even at 2 mA cm⁻² for 2 mAh cm⁻² of Li, NiCoON/NF still retains a high CE of 97% over 200 cycles [[Figure 3G](#)]. In strong contrast, NiCoO/NF only maintains a stable state for 60 cycles and drops suddenly. Apparently, bare NF also experiences severe disturbances and faster drops, which are mainly attributed to the internal short circuit of the cell caused by Li dendrite formation. Electrochemical impedance spectroscopy measurements were also implemented to study the charge transfer resistance after one cycle. As displayed in [Figure 3H](#), NiCoON/NF shows a significantly smaller charge transfer resistance than NiCoO/NF and bare NF, which confirms the outstanding Li plating and stripping kinetics and stable electrode interface. Therefore, these satisfactory results indicate that the higher electrical conductivity and better lithiophilicity of the NiCoON/NF nanoarrays largely reduce the Li nucleation barrier and facilitate the homogeneous Li plating/stripping.

Next, galvanostatic cycling tests based on symmetrical cells were carried out to explore the long-term plating/stripping stability at different current densities and capacities. [Figure 4A](#) displays the voltage-time profiles of NiCoON/NF, NiCoO/NF and NF at 1 mA cm⁻² with a fixed deposition capacity of 1 mAh cm⁻². Although both NiCoON/NF and NiCoO/NF present ultrastable cycling, the voltage hysteresis value of NiCoON/NF (23 mV) is lower than that of NiCoO/NF (26 mV), running over 1000 h without obvious potential oscillation. As a control, bare NF undergoes larger voltage hysteresis (30 mV) and irregular potential fluctuation appears only for 400 h due to the emergence of Li dendrites. At a current density of 5 mA cm⁻², the remarkable electrochemical stability of NiCoON/NF is still evident with a relatively low overpotential of 65 mV for 150 h, while NiCoO/NF and NF illustrate a short cycle life of 120 h with poor

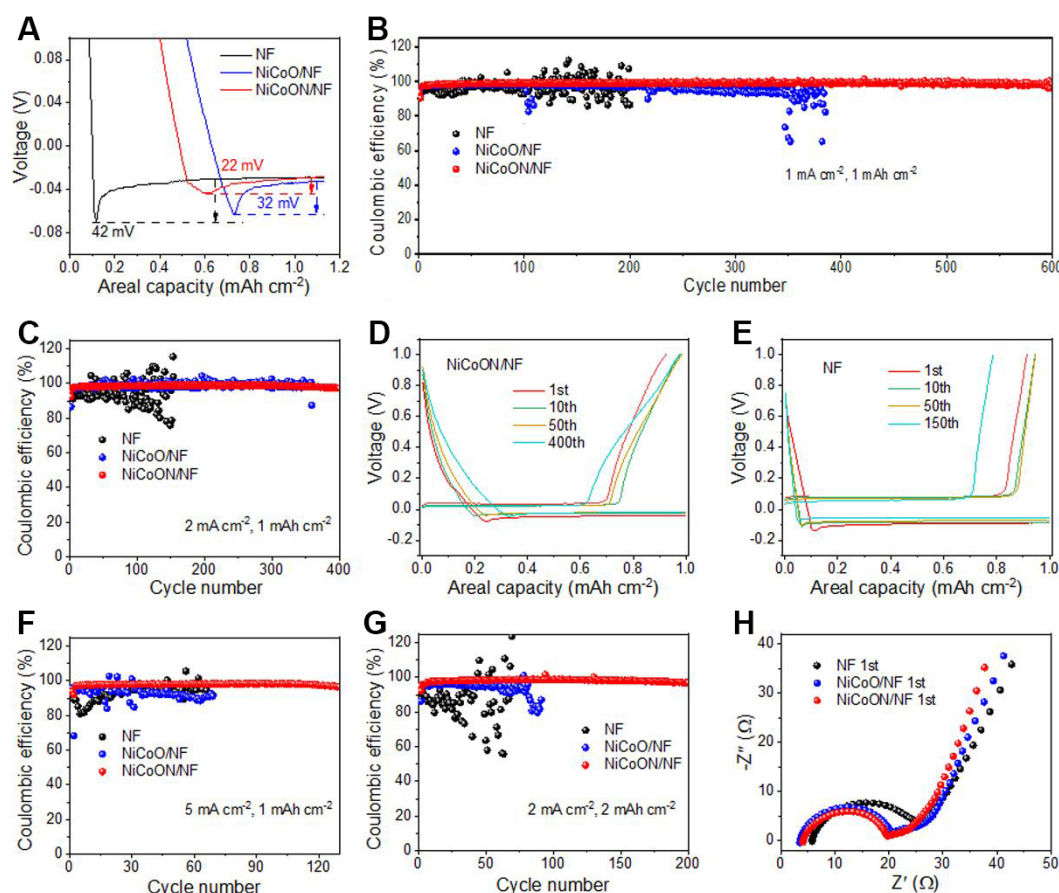


Figure 3. (A) Voltage profiles of nucleation overpotentials on different electrodes at 1 mA cm^{-2} . Comparison of CEs on NF, NiCoO/NF and NiCoON/NF current collectors with a fixed capacity of 1 mAh cm^{-2} at (B) 1 mA cm^{-2} , (C) 2 mA cm^{-2} and (F) 5 mA cm^{-2} and (G) CE at 2 mA cm^{-2} with 2 mAh cm^{-2} . (D, E) Corresponding discharge-charge curves on NiCoON/NF and NF at 2 mA cm^{-2} with 1 mAh cm^{-2} . (H) Electrochemical impedance spectroscopy (EIS) after 1st cycle at 1 mA cm^{-2} . CE: Coulombic efficiency.

variability [Figure 4B], suggesting an unstable SEI layer and internal short circuit induced by aggravated Li dendrite formation. Moreover, even with a high capacity of 3 mAh cm^{-2} at 1 mA cm^{-2} [Figure 4C], NiCoON/NF still retains a conspicuous cyclability with an ultralong cycling life (2000 h) and ultralow overpotential ($\sim 20 \text{ mV}$), implying excellent electrochemical performance among the different 3D current collectors, as presented in Supplementary Table 2. However, the bare NF decays quickly with increased overpotential. The remarkably advanced cycling performance of NiCoON/NF can be ascribed to the nitrogen-implanted nanoarray architecture with enhanced conductivities and superior Li_3N from the lithiation conversion enriched SEI layer, which can promote reduced voltage hysteresis and homogeneous Li deposition/dissolution.

Lithium deposition behavior

The Li metal deposition morphology on NF, NiCoO/NF and NiCoON/NF is also systematically evaluated via *ex-situ* SEM. As shown in Figure 5A, after depositing 1 mAh cm^{-2} of Li onto the NF electrode, Li tends to sparsely and locally nucleate in the early stages. As the amount of Li deposition increases from 1 to 5 and 15 mAh cm^{-2} , visible protuberances and cotton-like lithium dendrites accumulate along the NF skeleton [Figure 5B and C]. There is no doubt that the poor affinity of the NF host for Li aggravates the random nucleation of lithium, thereby facilitating the growth of dendrites. Moreover, the cross-sectional SEM image shows that the lithiophobicity of the Ni foam limits the internal deposition of lithium, resulting in a large

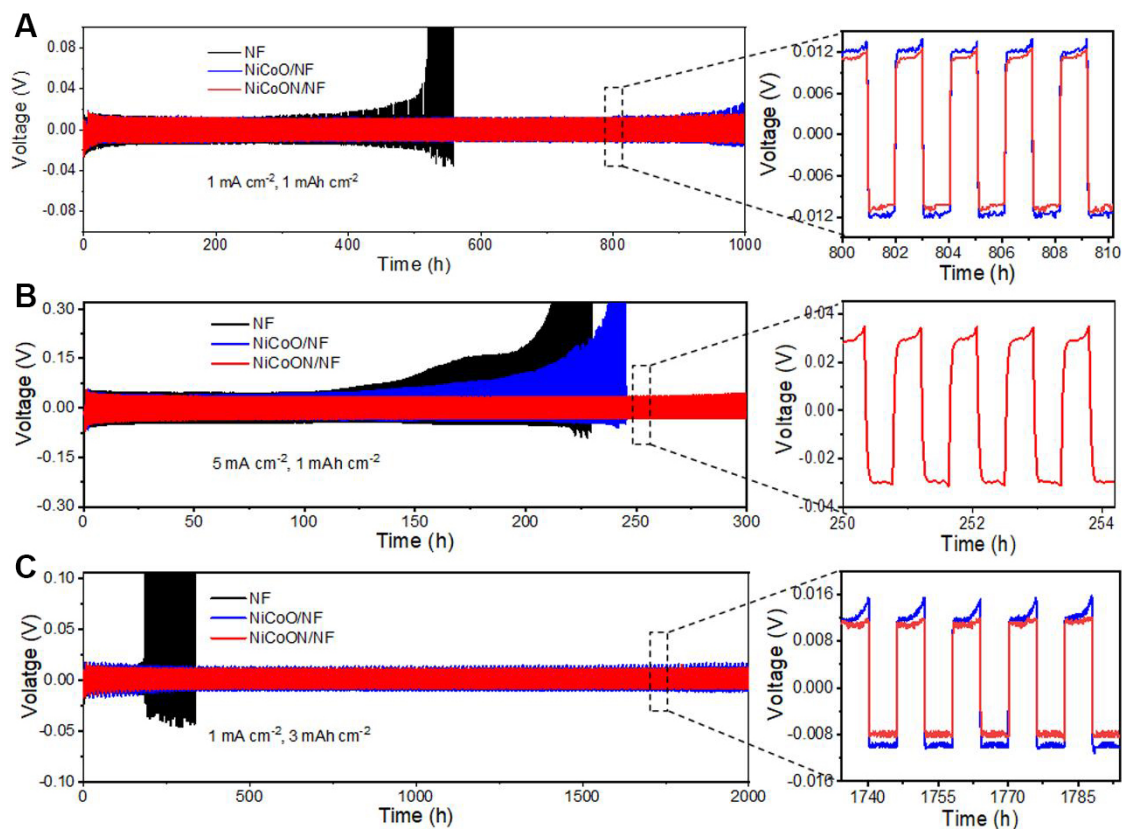


Figure 4. Long-term cycling performance of symmetrical batteries under different current densities and deposition capacities: (A) 1 mA cm^{-2} with 1 mAh cm^{-2} ; (B) 5 mA cm^{-2} with 1 mAh cm^{-2} ; (C) 1 mA cm^{-2} with 3 mAh cm^{-2} .

amount of dendrites remaining on the top [Figure 5D].

Compared to the bare NF, Li is preferentially plated on the lithiophilic surface of NiCoO/NF as a result of the efficacious surface area of dense nanorod-on-nanosheet arrays and more Li nucleation sites. With increasing Li from 1 to 5 and 15 mAh cm^{-2} , the growth of Li dendrites is largely controlled. However, inhomogeneous Li deposition and a small amount of dendrites are still unavoidable, which may be related to the low conductivity of the metal oxide [Figure 5E-G]. The cross-sectional SEM image in Figure 5H is consistent with this discussion. Li can enter the skeleton of NiCoO/NF, while there are still large chunks of Li deposits. Notably, the NiCoON/NF exhibits no visible lithium dendrites under various capacities of 1, 5 and 15 mAh cm^{-2} [Figure 5I-K]. After depositing Li at 1 mAh cm^{-2} , Li uniformly enters the dense skeleton of NiCoON/NF, owing to the sufficient lithiophilic nucleation sites. Under deep plating conditions from 5 to 15 mAh cm^{-2} , the wide internal space and ample pores of NiCoON/NF are gradually filled due to the cooperative action of enhanced surface lithophilicity and electrical conductivity, resulting in good Li nucleation and deposition. In particular, Li is uniformly deposited inside the 3D porous framework with the original thickness and no obvious lithium dendrites are found [Figure 5L]. These morphological results indicate that NiCoON/NF, as an ideal host, can provide enhanced surface lithophilicity for inducing uniform nucleation, thereby promoting the formation of dense lithium deposition.

To clarify the underlying mechanism, XRD analysis of Li@NiCoON/NF obtained after depositing 1 mAh cm^{-2} of lithium was performed. These peaks have a positive effect on the dense Li deposition due to the form of Li_3N and Li_2O [Supplementary Figure 11]^[40]. XPS was also performed to further confirm the

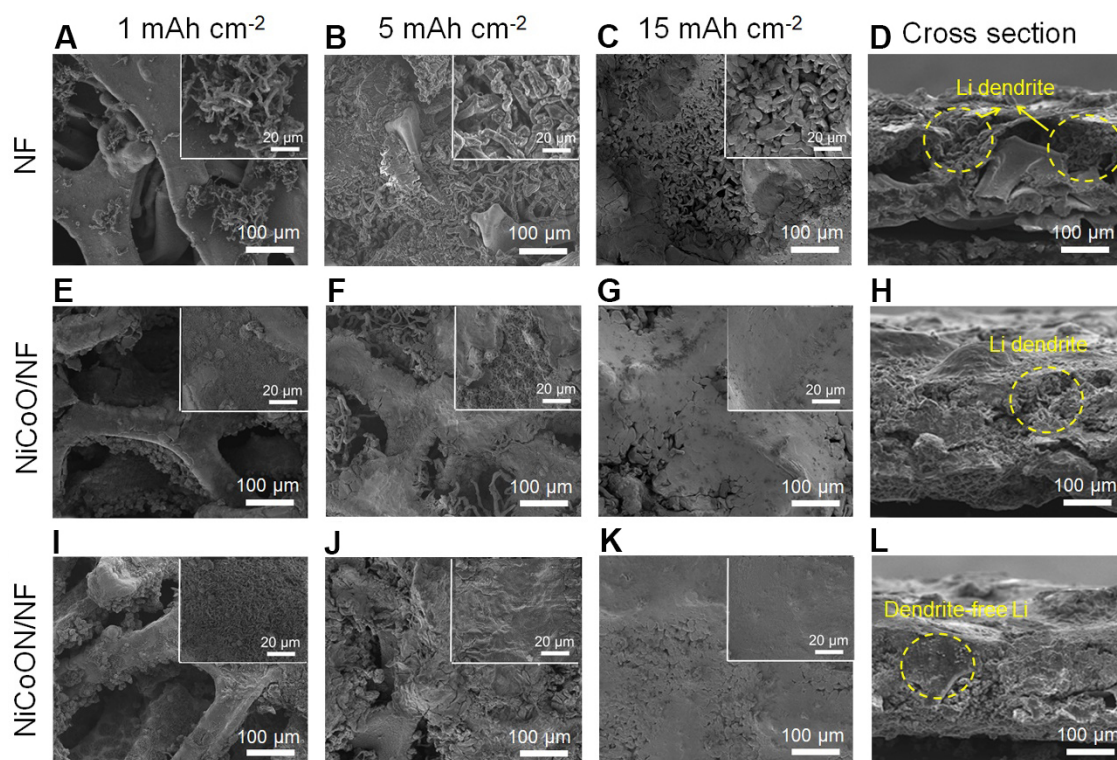


Figure 5. Top-view SEM images of Li deposition with 1, 5 and 15 mAh cm⁻² at 1 mA cm⁻²: (A-C) NF; (E-G) NiCoO/NF; (I-K) NiCoON/NF. Cross-sectional SEM images of Li deposition with 15 mAh cm⁻²: (D) NF; (H) NiCoO/NF; (L) NiCoON/NF. SEM: Scanning electron microscopy.

chemical composition change after lithiation in [Supplementary Figure 12](#). The three peaks at 55.1, 55.8 and 56.7 eV correspond to Li₂O, Li₃N and LiF, respectively^[41]. In addition, the N 1s spectrum includes three peaks at 399.7, 404.2 and 407.7 eV, attributed to Li₃N, LiNO₂ and LiNO₃, respectively^[42]. This result indicates the formation of a stable SEI film rich in Li₃N and Li₂O. After lithiation, the 3D structure and nanorod-on-nanosheet morphology are maintained, suggesting uniform Li deposition [[Supplementary Figure 13](#)]. The corresponding EDS elemental mapping of Li@NiCoON/NF confirms the homogeneous distribution of elemental Ni, Co, O and N, indicating the successful formation of Li₂O and Li₃N. The unique 3D NiCoON/NF nanoarrays combining a large surface area and enhanced lithiophilicity have the ability to strategically weaken the local current density and ensure the successful suppression of Li dendrites. Furthermore, the *in-situ* formed Li₂O and Li₃N layer with higher Li-ion conductivity further decreases the overpotential and induces Li deposition.

The morphological changes are also evaluated to realize the Li plating/stripping behavior on the NiCoON/NF and bare NF at 1 mA cm⁻² under the areal capacity of 1 mAh cm⁻². After the first electroplating, the surface of NF covers massive scattered dendritic lithium [[Figure 6A](#)], while metallic Li can enter the lithiophilic surface of NiCoON/NF [[Figure 6D](#)]. After stripping, moss-like Li remains on the NF surface [[Figure 6G](#)], while Li can be uniformly removed from NiCoON/NF [[Figure 6J](#)]. During the subsequent 50th plating/stripping, a significant amount of thick and loose Li is deposited on the NF [[Figure 6B](#)] and needle-like dead lithium is retained upon the 50th stripping [[Figure 6H](#)]. In sharp contrast, the NiCoON/NF architecture could spatially direct uniform lithium distribution along the 3D matrix and vertical nanoarrays could be clearly exposed again after Li stripping [[Figure 6E](#) and [K](#)]. After 100 cycles, the deposited lithium becomes worse [[Figure 6C](#)] and a significant quantity of lumped dead lithium

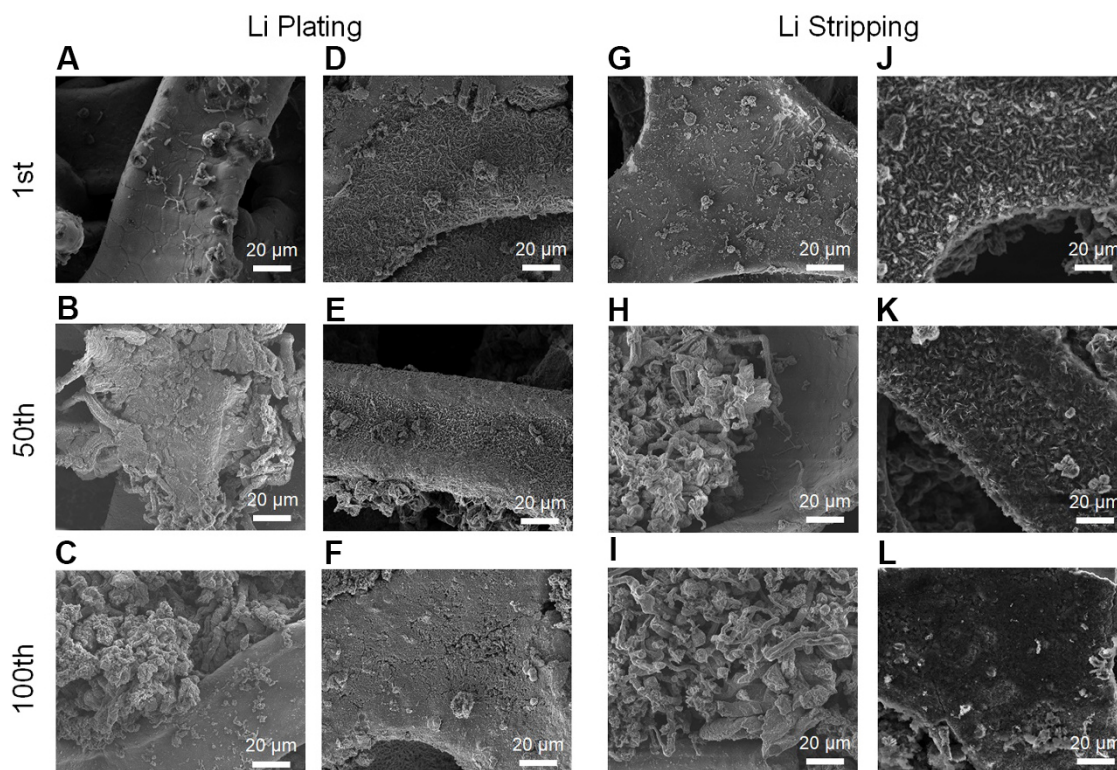


Figure 6. Li metal plating (A-C) and stripping morphologies (G-I) of NF at 1st, 50th and 100th cycles, respectively. Li metal plating (D-F) and stripping morphologies (J-L) of NiCoON/NF at 1st, 50th and 100th cycles, respectively.

accumulates on the bare body of NF after stripping [Figure 6I]. Such poor lithium deposition and the exfoliated dendritic morphology are responsible for the poor CE. Satisfactorily, Li is uniformly deposited on the NiCoON/NF and produces a dense flat Li layer [Figure 6F]. After Li stripping, the NiCoON/NF still maintains a comparatively clean and flat surface [Figure 6L], confirming its outstanding reversibility. These results indicate that NiCoON/NF can effectively hinder the dendrite growth and acquire more compact Li plating/stripping morphologies, which stem from the large specific surface area and promising lithiophilic properties.

Electrochemical properties of full cells

To evaluate the practicality of the NiCoON/NF current collector, full cells were assembled and tested by pre-depositing Li onto NF, NiCoO/NF and NiCoON/NF to obtain Li@NF, Li@NiCoO/NF and Li@NiCoON/NF, respectively, as anodes with LiFePO₄ as the cathode. Figure 7A illustrates the long-term cycling properties of full devices at 1 C (160 mA g⁻¹). Li@NiCoON/NF-LFP achieves improved cycling behavior with a maximum reversible capacity of 119 mAh g⁻¹ over 400 cycles, corresponding to a superior capacity retention of 85%. In comparison, Li@NiCoO/NF-LFP delivers a relatively reduced discharge capacity of 88.8 mAh g⁻¹ over 400 cycles with a poor capacity retention of 66.8%. However, the Li@NF-LFP experiences faster capacity degradation over 100 cycles with a capacity retention of only 34.9%, which is mainly introduced by inhomogeneous Li plating and fast SEI depletion. According to the corresponding charge/discharge profiles of the three full cells at the 100th cycle, Li@NiCoON/NF-LFP exhibits the lowest voltage polarization, indicating its good ability to inhibit Li dendrites [Figure 7B]. Li@NiCoON/NF-LFP also exhibits a better rate performance and a high discharge capacity, especially at a high current density of 5 C [Figure 7C]. However, Li@NiCoO/NF-LFP and Li@NF-LFP present obviously lower capacities at the same rate. In addition, the voltage polarization of the Li@NiCoON/NF-LFP cell is less than that of the

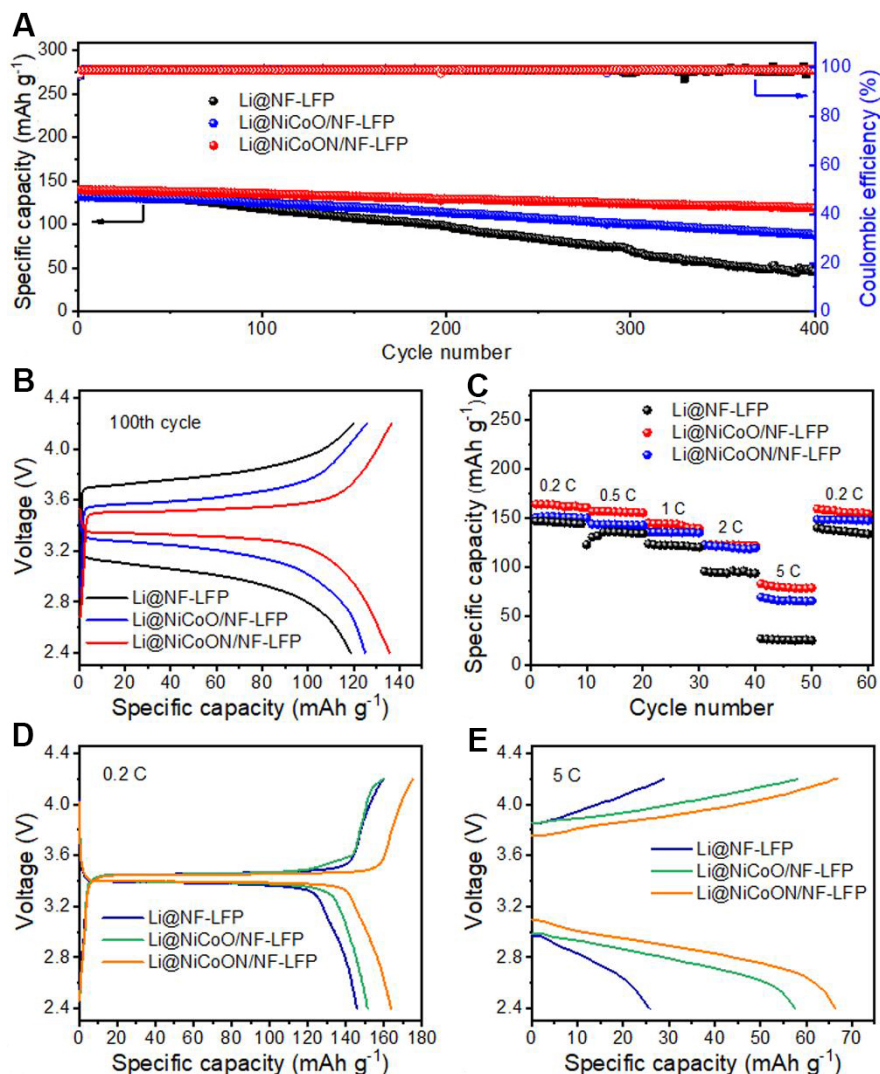


Figure 7. (A) Cycling performance of full cells with different Li anodes at 1 C (160 mA g⁻¹). (B) Comparison of full cells in voltage profiles at 100th cycle. (C) Rate capability. (D, E). Comparison of full cells in voltage hysteresis at 0.2 C and 5 C.

Li@NiCoO/NF-LFP and Li@NF-LFP cells at 0.2 C and 5 C, indicating the excellent electrochemical kinetics during the discharge and charge process [Figure 7D and E]. These encouraging results can be partially attributed to the superior lithiophilicity of the NiCoON/NF nanoarrays.

CONCLUSION

In summary, hierarchical Ni- and Co-based oxynitride nanoarrays with superior lithiophilicity have been constructed as stable hosts for uniform lithium deposition. The well-arranged nanoarrays with oxygen vacancies can offer high electronic conductivity and increased surface area to delocalize the practical current density and homogenize the Li-ion flux. Importantly, the *in-situ* formed Li₃N by the conversion reaction of NiCoON (i.e., NiCoO₂/CoO/Ni₃N) and Li can enhance the electron/ion conductivity for the kinetic induction of the homogeneous deposition of Li. Consequently, a promising Coulombic efficiency of 98.4% up to 600 cycles at 1 mA cm⁻² and an ultralong cycling life of 2000 h with a reduced voltage hysteresis under a high deposition capacity of 3 mAh cm⁻² have been achieved. Furthermore, Li@NiCoON/NF-LFP full cells also exhibit extraordinary electrochemical performance. This work illustrates the potential advantages of

Ni- and Co-based oxynitrides in the preparation of stable and dendrite-free lithium anodes to achieve safe and high-energy batteries.

DECLARATIONS

Acknowledgments

The authors thank M. Braun Intergas Systems Co., Ltd., Munich, Germany and Nanjing Mojiesi Energy Tech. Co., Ltd. for providing glove boxes and electrolyte, respectively.

Authors' contributions

Made substantial contributions to conception and design of the study and performed data analysis and interpretation: Wang Y, Zhu J, Duan X

Performed data acquisition, as well as provided administrative, technical, and material support: Xu H, Zhong J, Wang T, Lu B

Availability of data and materials

Not applicable.

Financial support and sponsorship

This work was financially supported by National Natural Science Foundation of China (No. 52074113; No. 22005091; No. 22005092), the Fundamental Research Funds of the Central Universities (No. 531107051048). We also acknowledge the support from the Hunan Key Laboratory of Two-Dimensional Materials (No. 2018TP1010), the Innovative Research Groups of Hunan Province (Grant 2020JJ1001), the Natural Science Foundation of Hunan Province, China (No. 2021JJ40046).

Conflicts of interest

All authors declared that there are no conflicts of interest.

Ethical approval and consent to participate

Not applicable.

Consent for publication

Not applicable.

Copyright

© The Author(s) 2021.

REFERENCES

1. Zhang Y, Ang EH, Yang Y, Ye M, Du W, Li CC. Interlayer chemistry of layered electrode materials in energy storage devices. *Adv Funct Mater* 2021;31:2007358. [DOI](#)
2. He W, Liu P, Qu B, et al. Uniform Na⁺ doping-induced defects in Li- and Mn-rich cathodes for high-performance lithium-ion batteries. *Adv Sci (Weinh)* 2019;6:1802114. [DOI](#) [PubMed](#) [PMC](#)
3. Yang Y, Zhu H, Xiao J, et al. Achieving ultrahigh-rate and high-safety Li⁺ storage based on interconnected tunnel structure in micro-size niobium tungsten oxides. *Adv Mater* 2020;32:e1905295. [DOI](#) [PubMed](#)
4. Ou X, Zhang G, Zhang S, Tong X, Tang Y. Simultaneously pre-alloying and artificial solid electrolyte interface towards highly stable aluminum anode for high-performance Li hybrid capacitor. *Energy Storage Mater* 2020;28:357-63. [DOI](#)
5. Wu C, Huang H, Lu W, et al. Mg doped Li-LiB alloy with in situ formed lithiophilic LiB skeleton for lithium metal batteries. *Adv Sci (Weinh)* 2020;7:1902643. [DOI](#) [PubMed](#) [PMC](#)
6. Guo J, Zhao S, Yang H, Zhang F, Liu J. Electron regulation enabled selective lithium deposition for stable anodes of lithium-metal batteries. *J Mater Chem A* 2019;7:2184-91. [DOI](#)
7. Kang H, Song M, Yang M, Lee J. Lithium metal anode with lithium borate layer for enhanced cycling stability of lithium metal batteries. *J Power Sources* 2021;485:229286. [DOI](#)
8. Liu S, Wang X, Xie D, et al. Recent development in lithium metal anodes of liquid-state rechargeable batteries. *J Alloys Compd* 2018;730:135-49. [DOI](#)

9. Shi Y, Wan J, Liu GX, et al. Interfacial evolution of lithium dendrites and their solid electrolyte interphase shells of quasi-solid-state lithium-metal batteries. *Angew Chem Int Ed Engl* 2020;59:18120-5. [DOI](#) [PubMed](#)
10. Tikekar MD, Choudhury S, Tu Z, Archer LA. Design principles for electrolytes and interfaces for stable lithium-metal batteries. *Nat Energy* 2016;1. [DOI](#)
11. Hou G, Ci C, Salpekar D, et al. Stable lithium metal anode enabled by an artificial multi-phase composite protective film. *J Power Sources* 2020;448:227547. [DOI](#)
12. Wang G, Xiong X, Xie D, et al. Suppressing dendrite growth by a functional electrolyte additive for robust Li metal anodes. *Energy Storage Mater* 2019;23:701-6. [DOI](#)
13. Chu F, Hu J, Wu C, et al. Metal-organic frameworks as electrolyte additives to enable ultrastable plating/stripping of Li anode with dendrite inhibition. *ACS Appl Mater Interfaces* 2019;11:3869-79. [DOI](#) [PubMed](#)
14. Liang J, Chen Q, Liao X, et al. A nano-shield design for separators to resist dendrite formation in lithium-metal batteries. *Angew Chem Int Ed Engl* 2020;59:6561-6. [DOI](#) [PubMed](#)
15. Ren W, Zheng Y, Cui Z, Tao Y, Li B, Wang W. Recent progress of functional separators in dendrite inhibition for lithium metal batteries. *Energy Storage Mater* 2021;35:157-68. [DOI](#)
16. Hatzell KB, Chen XC, Cobb CL, et al. Challenges in lithium metal anodes for solid-state batteries. *ACS Energy Lett* 2020;5:922-34. [DOI](#)
17. Krauskopf T, Richter FH, Zeier WG, Janek J. Physicochemical concepts of the lithium metal anode in solid-state batteries. *Chem Rev* 2020;120:7745-94. [DOI](#) [PubMed](#)
18. Dong T, Zhang J, Xu G, et al. A multifunctional polymer electrolyte enables ultra-long cycle-life in a high-voltage lithium metal battery. *Energy Environ Sci* 2018;11:1197-203. [DOI](#)
19. Lin Z, Guo X, Wang Z, et al. A wide-temperature superior ionic conductive polymer electrolyte for lithium metal battery. *Nano Energy* 2020;73:104786. [DOI](#)
20. Zhang R, Li NW, Cheng XB, Yin YX, Zhang Q, Guo YG. Advanced micro/nanostructures for lithium metal anodes. *Adv Sci (Weinh)* 2017;4:1600445. [DOI](#) [PubMed](#) [PMC](#)
21. Park S, Jin HJ, Yun YS. Advances in the design of 3D-structured electrode materials for lithium-metal anodes. *Adv Mater* 2020;32:e2002193. [DOI](#) [PubMed](#)
22. Li K, Hu Z, Ma J, Chen S, Mu D, Zhang J. A 3D and stable lithium anode for high-performance lithium-iodine batteries. *Adv Mater* 2019;31:e1902399. [DOI](#) [PubMed](#)
23. Zhang J, Zhou Y, Tu F, et al. In situ constructing lithiophilic and Ion/Electron dual-regulated current collector for highly stable lithium metal batteries. *Chem Eng J* 2022;428:132510. [DOI](#)
24. Lu W, Wu C, Wei W, Ma J, Chen L, Chen Y. Lithiophilic NiO hexagonal plates decorated Ni collector guiding uniform lithium plating for stable lithium metal anode. *J Mater Chem A* 2019;7:24262-70. [DOI](#)
25. Wang Z, Cheng D, He H, Zhou K. Hierarchical nanosheet arrays of metal oxides guide uniform deposition for lithium anodes. *ACS Sustainable Chem Eng* 2020;8:102-10. [DOI](#)
26. Huang X, Feng X, Zhang B, et al. Lithiated NiCo₂O₄ nanorods anchored on 3D nickel foam enable homogeneous Li plating/stripping for high-power dendrite-free lithium metal anode. *ACS Appl Mater Interfaces* 2019;11:31824-31. [DOI](#) [PubMed](#)
27. Chang X, Zhou X, Ou X, Lee C, Zhou J, Tang Y. Ultrahigh nitrogen doping of carbon nanosheets for high capacity and long cycling potassium ion storage. *Adv Energy Mater* 2019;9:1902672. [DOI](#)
28. Park H, Kwon J, Song T, Paik U. Lithiophilic surface treatment of metal- and metallic compound-based frameworks by gas nitriding for lithium metal batteries. *J Power Sources* 2020;477:228776. [DOI](#)
29. Luan J, Zhang Q, Yuan H, et al. Plasma-strengthened lithiophilicity of copper oxide nanosheet-decorated Cu foil for stable lithium metal anode. *Adv Sci (Weinh)* 2019;6:1901433. [DOI](#) [PubMed](#) [PMC](#)
30. Zhu J, Chen J, Luo Y, et al. Lithiophilic metallic nitrides modified nickel foam by plasma for stable lithium metal anode. *Energy Storage Mater* 2019;23:539-46. [DOI](#)
31. Lei M, You Z, Ren L, Liu X, Wang J. Construction of copper oxynitride nanoarrays with enhanced lithiophilicity toward stable lithium metal anodes. *J Power Sources* 2020;463:228191. [DOI](#)
32. Lei M, Wang JG, Ren L, et al. Highly lithiophilic cobalt nitride nanobrush as a stable host for high-performance lithium metal anodes. *ACS Appl Mater Interfaces* 2019;11:30992-8. [DOI](#) [PubMed](#)
33. Li Y, Hu L, Zheng W, et al. Ni/Co-based nanosheet arrays for efficient oxygen evolution reaction. *Nano Energy* 2018;52:360-8. [DOI](#)
34. Zhao D, Dai M, Liu H, et al. Sulfur-induced interface engineering of hybrid NiCo₂O₄@NiMo₂S₄ structure for overall water splitting and flexible hybrid energy storage. *Adv Mater Interfaces* 2019;6:1901308. [DOI](#)
35. Wang H, Hsu Y, Chen R, Chan T, Chen HM, Liu B. Ni³⁺-induced formation of active NiOOH on the spinel Ni-Co oxide surface for efficient oxygen evolution reaction. *Adv Energy Mater* 2015;5:1500091. [DOI](#)
36. Xu K, Chen P, Li X, et al. Metallic nickel nitride nanosheets realizing enhanced electrochemical water oxidation. *J Am Chem Soc* 2015;137:4119-25. [DOI](#) [PubMed](#)
37. Bao J, Zhang X, Fan B, et al. Ultrathin spinel-structured nanosheets rich in oxygen deficiencies for enhanced electrocatalytic water oxidation. *Angew Chem* 2015;127:7507-12. [DOI](#) [PubMed](#)
38. Cai Z, Bi Y, Hu E, et al. Single-crystalline ultrathin Co₃O₄ nanosheets with massive vacancy defects for enhanced electrocatalysis. *Adv Energy Mater* 2018;8:1701694. [DOI](#)
39. Xu L, Jiang Q, Xiao Z, et al. Plasma-engraved Co₃O₄ nanosheets with oxygen vacancies and high surface area for the oxygen evolution reaction. *Angew Chem Int Ed Engl* 2016;55:5277-81. [DOI](#) [PubMed](#)

40. Park K, Goodenough JB. Dendrite-suppressed lithium plating from a liquid electrolyte via wetting of Li_3N . *Adv Energy Mater* 2017;7:1700732. [DOI](#)
41. Wang Y, Zhang W, Qi Y, et al. Uniform titanium nitride decorated Cu foams by electrophoretic deposition for stable lithium metal anodes. *J Alloys Compd* 2021;874:159916. [DOI](#)
42. Yan C, Yao YX, Chen X, et al. Lithium nitrate solvation chemistry in carbonate electrolyte sustains high-voltage lithium metal batteries. *Angew Chem Int Ed Engl* 2018;57:14055-9. [DOI](#) [PubMed](#)